Scaling analysis of diffusion-mediated island growth in surface adsorption processes

M. C. Bartelt
Institute for Physical Research and Technology, Iowa State University, Ames, Iowa 50011

J. W. Evans
Department of Mathematics, Iowa State University, Ames, Iowa 50011
and Ames Laboratory, Iowa State University, Ames, Iowa 50011
(Received 19 May 1992)

We examine the competition between diffusion-mediated irreversible nucleation and growth of islands during submonolayer deposition on perfect substrates. We provide a detailed scaling theory for the complete distribution of island sizes and separations, both with the ratio of diffusion to deposition rate and with time. Scaling functions and exponents are obtained by simulation. The leading scaling behavior is independent of details of the island structure. These results are supplemented by an analysis of rate equations for the island-size distribution whose unconventional form appropriately describes island nucleation and growth mechanisms. The exponents agree with the simulations and the island-size distribution shows qualitative agreement. We further provide simulation results for the scaling of the island-separation distribution, quantifying, in particular, the depletion in the concentration of pairs of islands at small separations.

I. INTRODUCTION

Recent scanning-tunneling-microscopy (STM) experiments clearly reveal the evolution of far-from-equilibrium structure during island-forming adsorption processes in various systems.[1,2] Here traditional quasiequilibrium nucleation and growth theories[3,4] must be replaced by appropriate far-from-equilibrium island-growth models and scaling theories.[5,6]

Specifically, in this report, we focus on processes involving adsorption on single-crystal surfaces, leading to diffusion-mediated nucleation and growth of islands. Adsorption achieved by molecular-beam or vapor deposition is effectively irreversible and random for the systems of interest here. In the traditional nucleation-mediated process, the rate-limiting step, for low island mobility and density, is typically the formation of clusters of some critical number of atoms s^* for which growth is more likely than decay; for sizes $s<s^*$, a quasiequilibrium holds.[3,4] It has been noted that often the adatom chemical potential may greatly exceed its equilibrium value, implying that s^* will be small.[3] Here, however, we adopt a kinetic viewpoint that island formation will often be effectively *irreversible*, guaranteeing far-from-equilibrium behavior.

This kinetic behavior is based on the feature that the activation energy barrier E_a^0 for single-atom diffusion will certainly be less than the minimum barrier $E_a=E_a^0+\delta E$ for escape of an atom from an island.[7] Thus, it is possible that there exists a range of temperatures T where the isolated adatom diffusion rate

$$h_0=\nu\exp(-E_a^0/k_BT)$$

is comparable to or dominates the deposition rate r while the rate

$$h_e\approx\nu\exp(-E_a/k_BT)$$

for escape from island edges is insignificant (relative to r). Judicious choice of r is, of course, required for this scenario. Clearly, the larger the δE, the broader this range. An alternative approach would be to select T so that $h_0\gg h_e$, and analyze island-density scaling with varying r.

We consider only the regime of *low* coverage where the finite extent of islands and their subsequent coalescence are not significant factors. For irreversible island formation, it is clear that the island density N decreases with increasing ratio of diffusion to deposition rates $D=h_0/r$. As D increases, deposited adatoms or "walkers" can on average travel farther between deposition events. One expects a scaling relation[1,6] of the form $N\sim D^{-\chi}$ as $D\to\infty$ for fixed submonolayer coverages. Mo *et al.*[1] made the important observation that knowledge of this relation allows one to extract an estimate of E_a^0, from experimental STM data for the variation of N with T. Underlying this observation is the assumption that migration of adatoms can be effectively described by a pure random walk. Under this assumption, we develop here a complete description of the scaling of the full island-size distribution with both D and coverage θ (or dose time t). We further analyze the behavior of the distribution of island separations, as well as the effect of anisotropy in the diffusion rates.

Another basic issue, which we do not address in this report, is that of the structure of the irreversibly formed growing islands. Their structure could assume the equilibrium form, if island restructuring is efficient on the time scale of deposition; one could observe nonequilibrium "growth figures" if restructuring is incomplete,[8] or even dendritic or diffusion-limited-aggregation (DLA-like) fractal aggregates if restructuring is highly restricted.[2,9] The latter behavior derives from the Mullins-Sekerka shape instability associated with walkers deposited on the substrate diffusing to the island edges and ir-

reversibly aggregating. It should be noted that for higher coverages, deposition on top of the islands will be significant. Island growth resulting from such atoms diffusing to and incorporating at island edges results in an anti-DLA shape stabilization of island structure, growth occurring preferentially at indentations or fjords.[10] Also for fractal islands, deposition directly in the fjords at higher coverages will lead to significant thickening. This behavior has been observed experimentally.[2] Clearly, the details of island shape will be highly system specific. For this reason, we focus here on more universal size and separation scaling behavior.

We note that island-density scaling has been considered previously for adsorption models where island growth is incorporation rather than diffusion mediated. In island-forming chemisorption from an equilibrated physisorbed precursor, precursor density and, thus, chemisorption rates should be enhanced at island edges.[11] Thus the process involves a competition between birth of islands by chemisorption on empty regions of the substrate, and growth of existing islands by chemisorption at enhanced rates at their edges. The decrease of the island density with the ratio of birth to growth rates (at fixed coverage) has been elucidated in these "cooperative sequential adsorption" models.[12] In some cases, they reduce to Kolmogorov "grain-growth-type" models, where islands are born randomly at a constant rate and grow deterministically at a fixed velocity following nucleation.[13] More generally, scaling of the complete island-size distribution has been analyzed for a variety of models including droplet coalescence,[14] percolation,[15] and thin-film growth mechanisms.[16] A Smoluchowski rate-equation analysis has been used extensively in previous studies of nucleation and growth in thin-film systems,[3] and in some cases scaling theories developed.[16] However, no analysis of the rate equations appropriate for the problem we consider here was available prior to this study. We emphasize that even effective rate-equation analyses yield only qualitative information, since they systematically ignore fluctuations and correlations. In the absence of an exact microscopic solution, simulations are essential to study growth models and test scaling theories.

The outline of this work is as follows. In Sec. II we survey briefly recent experimental systems and findings, and in Sec. III we describe the details of our model and the simulations. The scaling relations are postulated and examined in Sec. IV. Section V is a summary of the simulation results, which should be compared with the rate-equation solutions presented in Sec. VI. Section VII addresses some of the scaling ideas and results for the island-separation distribution and short-range size-size correlations. Further investigation of these issues is postponed to a separate report. Finally, we conclude the discussion of our results in Sec. VIII.

II. APPLICATIONS TO SPECIFIC SYSTEMS

Studies of a few different experimental systems, grown under conditions that favor irreversible aggregation and low island mobility and dissolution, have been reported in the recent literature. Usually they involve real-space imaging (e.g., scanning tunneling and atomic force microscopy) and complementary surface-sensitive diffraction methods (e.g., low-energy electron diffraction). In the former, visual access to the spatial distribution and structure of the stable islands allows for direct scaling analysis of the average populations on the substrate, while in the latter the average distribution of island sizes and separations is reflected naturally in the structure of the diffracted intensity peaks, whose variation, e.g., with temperature, can be followed.

For systems of interest here, the most relevant issues are indeed the size and separation distributions of *two-dimensional* islands, and their evolution with system parameters and coverage. In their recent study, Mo *et al.* addressed the island-size scaling with D, in connection with STM studies of submonolayer (~ 0.1 ML) diffusion of Si atoms, during deposition on Si(001) surfaces. They observe stable Si dimer formation on wide surface terraces (100–1000 Å), and no significant escape of dimers or atoms from the Si islands, so effectively the islands form irreversibly. Diffusion on Si(001) is very anisotropic, and well modeled using properties of one-dimensional random walks. Direct account of the details of the interactions in the system, such as aspects of the bonding of the atoms to the islands (as they relate to the elongated shapes observed), do not affect strongly the island scaling, as concluded in Mo *et al.* from both experiments and simulations. In spite of the simplicity of the method they proposed, their results for diffusion barriers are similar to others obtained from *ab initio* calculations.[17]

Zhang, Lu, and Metiu[18] have made a detailed study of the energetic barriers for various diffusion processes in this system using a Stillinger-Weber potential. Indeed, they find that dimer motion and dissociation, as well as trimer dissociation, are extremely rare events. An atom adjacent to a dimer string may be captured by another atom to form a dimer in an adjacent row. This dimer then acts as the nucleus of an adjacent dimer string. In the STM counting of islands, it would thus be appropriate to identify adjacent dimer rows as a single island. Then, island formation is indeed effectively irreversible, and our scaling theory will apply. In passing, we note that Zhang, Lu, and Metiu propose a different mechanism from Mo *et al.* for the formation of elongated island shapes. However, since island dissolution is not involved, this discrepancy does not affect island-density scaling.

In another room-temperature STM study by Hwang *et al.*[2] of deposition of Au on Ru(0001), a dramatically far-from-equilibrium fractal structure of the growing Au islands was observed. This clearly demonstrates that island restructing is highly restricted, further implying that island dissolution is not possible at these temperatures. Annealing to 650 K produced significant island restructuring, but still *no* dissolution. Even at room temperature, the island density is quite low, reflecting high diffusion rates for isolated atoms. Thus this system is a good candidate to study the scaling of the island density under conditions of irreversible aggregation. It should be noted that the width of the arms of these fractal Au islands is quite broad (~ 100 Å). A detailed analysis of the

rearrangement and diffusion mechanisms required to produce this width will be the subject of a separate investigation.

Finally, we describe a chemisorption system where our model and scaling ideas may be applicable. Extensive theoretical and experimental studies of H_2O adsorption on transition-metal surfaces show that surface diffusion of H_2O is rapid on the time scale of typical adsorption experiments (even at low temperatures). Under these conditions, water can rapidly form hydrogen-bonded clusters, even at low coverages (see Ref. 19 for a review of these systems). For H_2O adsorption on Ni(110), and possibly on other fcc(110) metals, there is evidence that the H_2O dimer is stable at low coverages, both to dissociation and to addition. The latter feature makes our model inapplicable. However, on many other metal surfaces [e.g., Ni(111), Cu(100), Pt(111)], there is no evidence of exclusive dimer formation. In fact, no significant population of dimers is observed. This is presumably because the high H_2O mobility at low coverages, and the strong hydrogen bonding interaction, lead to the rapid formation of larger clusters.[19]

III. THE MODEL AND SIMULATION ALGORITHM

We consider random deposition of particles on the empty sites of a lattice, at constant rate r, starting with a clean surface at $t=0$. Deposited particles can hop between neighboring empty sites, at constant rate h_0, until they meet other walkers or islands already formed on the surface. A cluster of two or more particles (an island) is *immobile* and structureless. Such islands occupy single sites, but can assume variable size. When a walker arrives at a site adjacent to another walker, it aggregates with that walker, converting it to an island of size two. When a walker arrives at a site adjacent to an isolated island of size $s \geq 2$, it aggregates with that island converting it to an island of size $s+1$. In the rare event (in the regime of large h_0) that a walker reaches a site with more than one neighbor occupied by an island or another walker, it aggregates with one of these chosen randomly but weighing by size. Aggregation is always irreversible and trapping occurs instantaneously.

We employ a "hybrid" simulation algorithm for optimum efficiency. At each stage we decide whether to attempt to deposit at a randomly chosen site or to move with certainty one of the walkers selected at random from a continually updated list of all walkers on the lattice. The former choice is made with probability $p_r = r/(r+h_0 n)$ and the latter with probability $p_h = 1-p_r$, where n denotes the actual density of walkers on the surface. Our algorithm is optimal in the sense that almost all attempts to deposit succeed since the island and walker densities are typically very low. (Selecting from an updated list of empty sites to guarantee adsorption would be inefficient.) On the other hand, since the walker density is so low, it is appropriate to keep a list of walkers in order to implement hopping. Time in the simulations is chosen consistent with the rate specifications.

Our simulations involved typically more than 200 runs on lattices of at least 10^5 sites, with periodic boundary conditions, and covered a range of diffusion ratios ($10^4 \leq D \leq 10^8$) and low coverages (<0.2 ML). A typical run takes between 15 min and an hour of CPU time (depending on the hopping rate) on a silicon graphics machine. For illustration, Fig. 1 shows typical

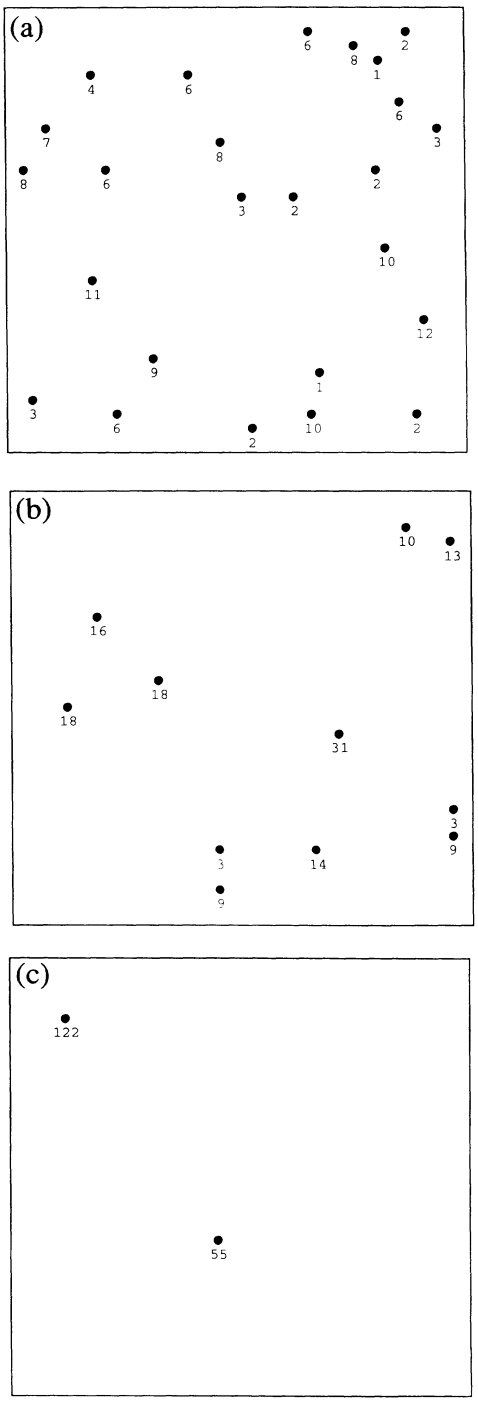

FIG. 1. Configuration of islands in a 30×30 window of a 600×600 simulation sample for isotropic diffusion. The dose is 15% in (a) $D=10^4$, (b) $D=10^6$, and (c) $D=10^8$. Note how fewer but larger and further separated islands are nucleated as D increases.

configurations from the simulation of two-dimensional isotropic diffusion.

As above, we will denote the average island density by N, and the walker density by n. Wherever it appears, d refers to the substrate dimensionality. The average area associated with an island is $A=1/N$, and in the regime where $n \ll N \ll 1$, $l=A^{1/d_w}$ gives the typical diffusion length (in unit lattice spacings). Here d_w denotes the "dimensionality" of the random-walk paths on the surface. Specifically, $d_w=2$ for isotropic diffusion, whereas $d_w=1$ in the strongly anisotropic case. The case of extreme anisotropy in surface migration is representative of the Si on Si(001) system, for instance, and, although not equivalent to, scales such as diffusion on a one-dimensional substrate (see Sec. V). In many real systems at low coverages, the dependence of the island-capture probabilities on the island size and shape is weak. In our model they are ignored for simplicity.

IV. THE SCALING THEORY

Let n_s denote the average density (per site) of islands of size s. Then the total average density of islands is $N=\sum_{s\geq 2} n_s$ and that of the walkers is $n=n_1$. The total dose, defined as the number of particles (per site) deposited until time t, is $\theta=\sum_{s\geq 1} s n_s$. One can measure the average island size (here size means number of particles incorporated) as the ratio

$$s_{\rm av}=\sum_{s\geq 1} s n_s \Big/ \sum_{s\geq 1} n_s=\theta/(n+N)\sim\theta/N \ ,$$

when $N \gg n$. Note that the most commonly used measure of the island size is a weighted average, usually the first moment of the distribution $s n_s$, namely

$$\bar{s}_{\rm av}=\sum_s s^2 n_s \Big/ \sum_s s n_s \ ,$$

but as regards the scaling with t and D, the choice is irrelevant, as the following shows. Note that the relation between $\bar{s}_{\rm av}$ and θ is not simple. We postulate that, for large D and all but short times, scaling holds as

$$n_{s\geq 1}\sim (rt)^{2\omega+1} D^{-2\chi} g[s(rt)^{\omega} D^{-\chi}] \ . \tag{1}$$

Specifically, in Appendix A, we show that the range of times over which the above scaling applies can actually be written as $rt_{\rm min}=D^{-|\chi/\omega|} \ll rt < O(1)$. Substituting (1) into the $s_{\rm av}$ and $\bar{s}_{\rm av}$ expressions gives

$$s_{\rm av}=\frac{\sum_{s=1}^{\infty} s n_s}{\sum_{s=1}^{\infty} n_s}\sim\frac{\int_0^{\infty} ds\, s (rt)^{2\omega+1} D^{-2\chi} g[s(rt)^{\omega} D^{-\chi}]}{\int_0^{\infty} ds\,(rt)^{2\omega+1} D^{-2\chi} g[s(rt)^{\omega} D^{-\chi}]}$$

$$\sim (rt)^{-\omega} D^{\chi}\frac{\int_0^{\infty} du\, u g(u)}{\int_0^{\infty} du\, g(u)} \ , \tag{2}$$

and

$$\bar{s}_{\rm av}=\frac{\sum_{s=1}^{\infty} s^2 n_s}{\sum_{s=1}^{\infty} s n_s}\sim\frac{\int_0^{\infty} ds\, s^2 (rt)^{2\omega+1} D^{-2\chi} g[s(rt)^{\omega} D^{-\chi}]}{\int_0^{\infty} ds\, s (rt)^{2\omega+1} D^{-2\chi} g[s(rt)^{\omega} D^{-\chi}]}$$

$$\sim (rt)^{-\omega} D^{\chi}\frac{\int_0^{\infty} du\, u^2 g(u)}{\int_0^{\infty} du\, u g(u)} \ . \tag{3}$$

Note that the argument of g scales like $s/s_{\rm av}$ or $s/\bar{s}_{\rm av}$. Also, since in our model the islands occupy single sites, regardless of their size, the total density of occupied sites is not θ but, rather, $n+N$.

From (1) it follows that $\theta\sim rt\int_0^{\infty} dx\, x g(x)$, and for the average densities,

$$N\sim (rt)^{\omega+1} D^{-\chi}\int_0^{\infty} dx\, g(x)$$

and (4)

$$n\sim (rt)^{-\alpha} D^{-\varphi} g(0) \ ,$$

as $D\to\infty$. Here $\alpha=-(2\omega+1)$ and $\varphi=2\chi$, given that $g(0)\neq 0$, as born out by our simulation results. Thus, the scaling in (1) applies to both immobile islands ($s\geq 2$) and mobile walkers ($s=1$). In this respect, the most important feature of the scaling function g is the fact that it does *not* vanish for small arguments. Also, given the monotonicity of N and n in the scaling region, the exponent ω must satisfy the inequality $-1<\omega<-\frac{1}{2}$. We focus on the analysis of the above scaling in the two important cases corresponding to (i) isotropic and (ii) (strongly) anisotropic diffusion on two-dimensional surfaces. Diffusion on a linear lattice scales with the same exponents as (ii), which are different from the exponents governing case (i). The relevant dimensionality is actually d_w.

We emphasize that the scaling theory presented in this work applies only to *low* coverages, where islands occupy a small fraction of the surface and direct interference between growing islands is insignificant. For real systems, with extended islands that occupy a finite fraction of the surface, deposition of particles on top of the islands and their subsequent migration to and aggregation at the island edges must be properly accounted for. Large islands may then compete favorably for the incoming particles and scaling must be modified to incorporated this size dependence in the growth rates. For higher coverages, when there is no impediment to island coalescence, the ideas developed in percolation theory are more useful. Scaling with respect to D and rt should be preserved, since coalescence simply rescales sizes. Specifically, one expects that $s_{\rm av}/s_* \sim (\theta-\theta_c)^{-\gamma}$, where θ_c is the percolation threshold[15] and $s_* \sim (rt)^{-\omega} D^{\chi}$. For our model the spatial correlations have finite range, so the exponent γ should have the random percolation value.

We have assumed that the nucleation of islands is homogeneous rather than defect mediated. For a small concentration of (pointlike) defects ε, which act as perfect walker traps, and for low-enough D, one has $N \gg \varepsilon$, and the presence of defects will not significantly affect the homogeneous scaling behavior. However, as D exceeds

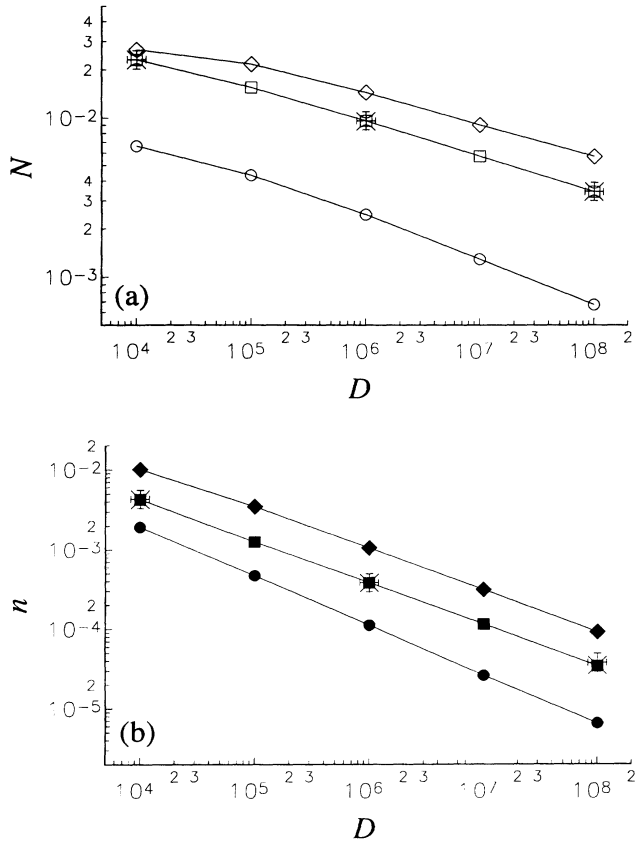

FIG. 2. The scaling of (a) the simulated average island density N and (b) walker density n with the relative diffusion constant D. Shown are the cases of isotropic diffusion (circles, $\theta=5\%$), infinitely anisotropic diffusion (boxes, $\theta=10\%$), in two dimensions, and the one-dimensional case (diamonds, $\theta=10\%$). In order to check for finite-size effects, we added, for the anisotropic case, data for a 1000×100 lattice (boxes), a $10\,000\times10$ lattice (crosses), and a $10\,000\times100$ lattice (multis).

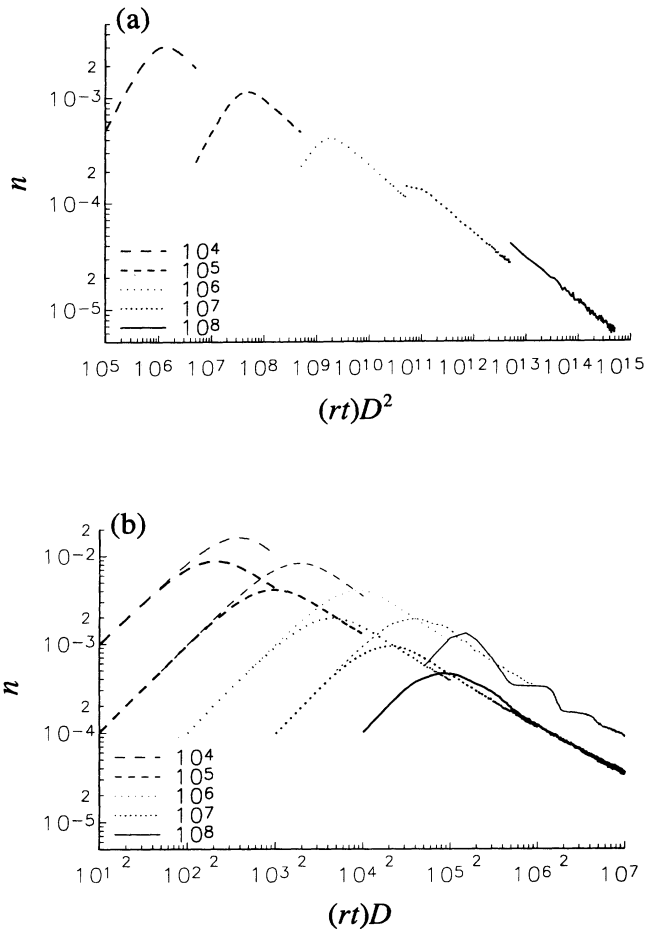

FIG. 4. Simulation results for the scaling in time of the average walker density n in the range $D=10^4-10^8$, for (a) isotropic, and (b) infinitely anisotropic diffusion (thick lines) in two dimensions, and the one-dimensional case (thin lines).

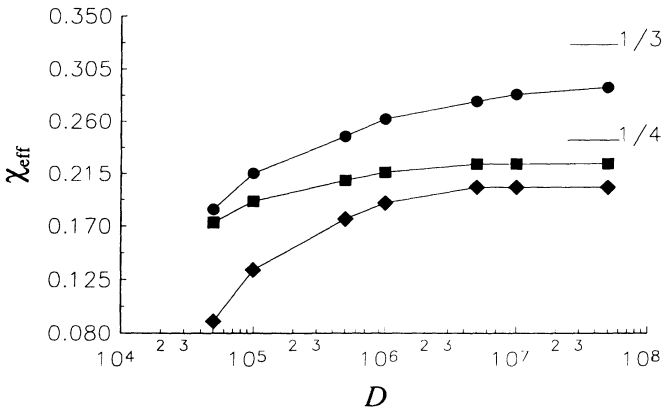

FIG. 3. The effective exponent χ_{eff} obtained from the simulations in the range $D=10^4-10^8$, for isotropic diffusion (●, $\theta=5\%$), infinitely anisotropic diffusion (■, $\theta=10\%$), in two dimensions, and the one-dimensional case (◆, $\theta=10\%$).

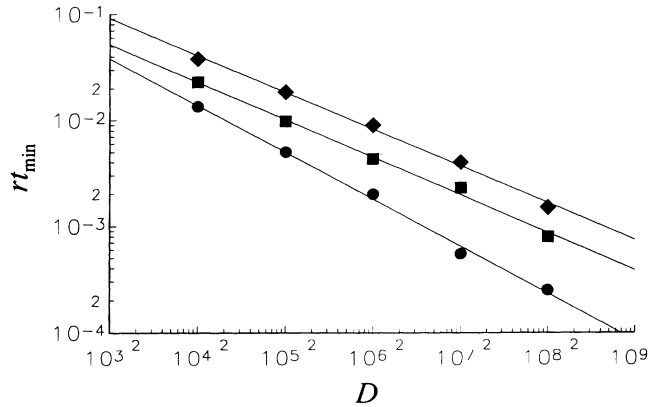

FIG. 5. The dependence of rt_{min} on the diffusion rate D at the onset of scaling. In two dimensions, ● denotes isotropic diffusion (slope, -0.44) and ■ denotes infinitely anisotropic diffusion (slope, -0.35). In one dimension, denoted by ◆ (slope: -0.34).

TABLE I. Simulation and rate-equation estimates of the exponents χ, φ, α, and ω, at fixed dose (5% for isotropic and 10% for infinitely anisotropic and one-dimensional diffusion), in the range $D=10^4-10^8$.

d	χ	φ	ω	α
1	0.25[a]	0.51[a]	−0.76[a]	0.48[a]
	$\frac{1}{4}$[b]	$\frac{1}{2}$[b]	$-\frac{3}{4}$[b]	$\frac{1}{2}$[b]
2 (anisotropic)	0.24[a]	0.52[a]	−0.75[a]	0.49[a]
	$\frac{1}{4}$[b]	$\frac{1}{2}$[b]	$-\frac{3}{4}$[b]	$\frac{1}{2}$[b]
2 (isotropic)	0.30[a]	0.62[a]	−0.67[a]	0.31[a]
	$\frac{1}{3}$[b]	$\frac{2}{3}$[b]	$-\frac{2}{3}$[b]	$\frac{1}{3}$[b]

[a]Simulations (±0.03).
[b]Rate equations.

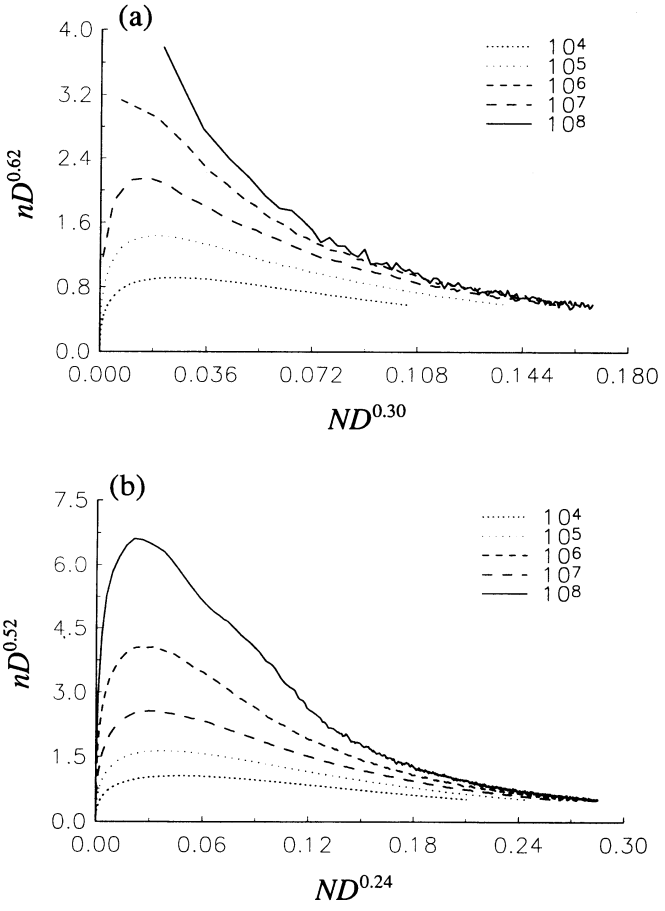

FIG. 6. The scaled walker density nD^{φ} vs the scaled island density ND^{χ} for (a) two-dimensional isotropic and (b) two-dimensional infinitely anisotropic diffusion. The curves show the initial increase in both n and N, and the crossover to a quasisteady (scaling) regime, where $dn/dt \sim 0$ and the asymptotic relations (a) $n \sim 1/(DN)$ and (b) $n \sim 1/(DN^2)$ hold.

$O(\varepsilon^{-1/\chi})$, (i.e., as ε exceeds the density of islands that would otherwise nucleate homogeneously), N will eventually cross over from the $D^{-\chi}$ behavior to a constant of order ε (as most islands are nucleated at the defects, whose initial spatial distribution also determines that of the formed islands).

V. SIMULATION RESULTS

Our simulation results are summarized as follows. On Fig. 2 we demonstrate the scaling behavior with D, of the average density of walkers, $n \sim D^{-\varphi}$, and islands,

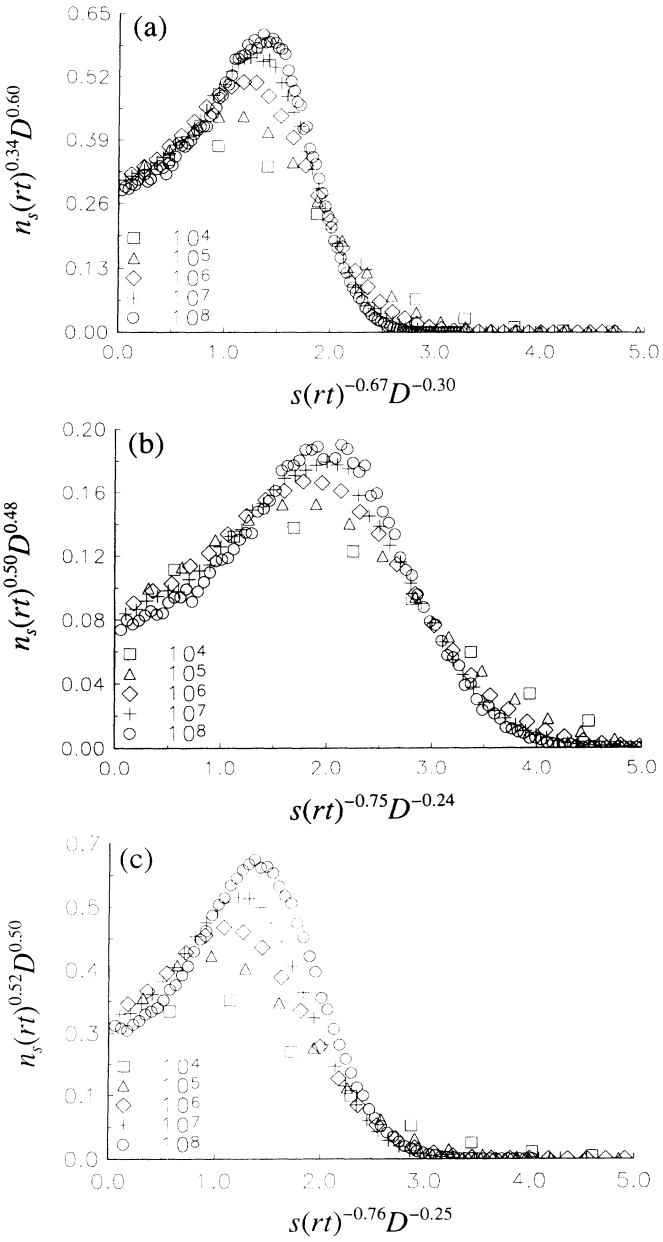

FIG. 7. Scaling of the island-size distribution with D, in the range $D=10^4-10^8$, for (a) isotropic ($rt=5\%$) and (b) infinitely anisotropic diffusion ($rt=10\%$) in two dimensions, and (c) the one-dimensional case with $rt=10\%$.

$N \sim D^{-\chi}$, at fixed dose. For $10^4 \le D \le 10^8$, one finds $N \sim (0.52 \pm 0.02) D^{(-0.25 \pm 0.03)}$ and $n = (1.23 \pm 0.02) D^{-(0.51 \pm 0.03)}$ for one-dimensional diffusion (at 0.1 ML), $N \sim (0.51 \pm 0.02) D^{-(0.24 \pm 0.03)}$ and $n = (0.77 \pm 0.02) D^{-(0.52 \pm 0.03)}$ for two-dimensional anisotropic diffusion (at 0.1 ML), and $N \sim (0.55 \pm 0.02) D^{-(0.30 \pm 0.03)}$ and $n \sim (0.92 \pm 0.02) D^{-(0.62 \pm 0.03)}$ for isotropic diffusion (at 0.05 ML). Thus in the range of finite $10^4 \le D \le 10^8$ one finds effective exponents, χ_{eff} and φ_{eff}, below the asymptotic values, which we assume are given by $\chi(d_w = 1) = \frac{1}{4}$, $\chi(d_w = 2) = \frac{1}{3}$, and $\varphi(d_w = 1) = \frac{1}{2}$, $\varphi(d_w = 2) = \frac{2}{3}$, in the scaling limit, $D \to \infty$. In a more refined analysis, effective exponents are determined as local slopes in appropriate log-log plots, as illustrated in Fig. 3 for the exponent χ. This is especially useful information in practice, since small deviations in χ can produce considerable shifts in the energy barrier estimates. Assuming Arrhenius behavior of the diffusion coefficient, the estimate for the energy barrier, obtained from the T dependence of

$$(1/\chi)\ln(N) \sim E_a^0 / k_B T \ ,$$

is sensitive to the choice of χ. The value used for this exponent when extracting E_a^0 should be the appropriate for the experimental range of D.

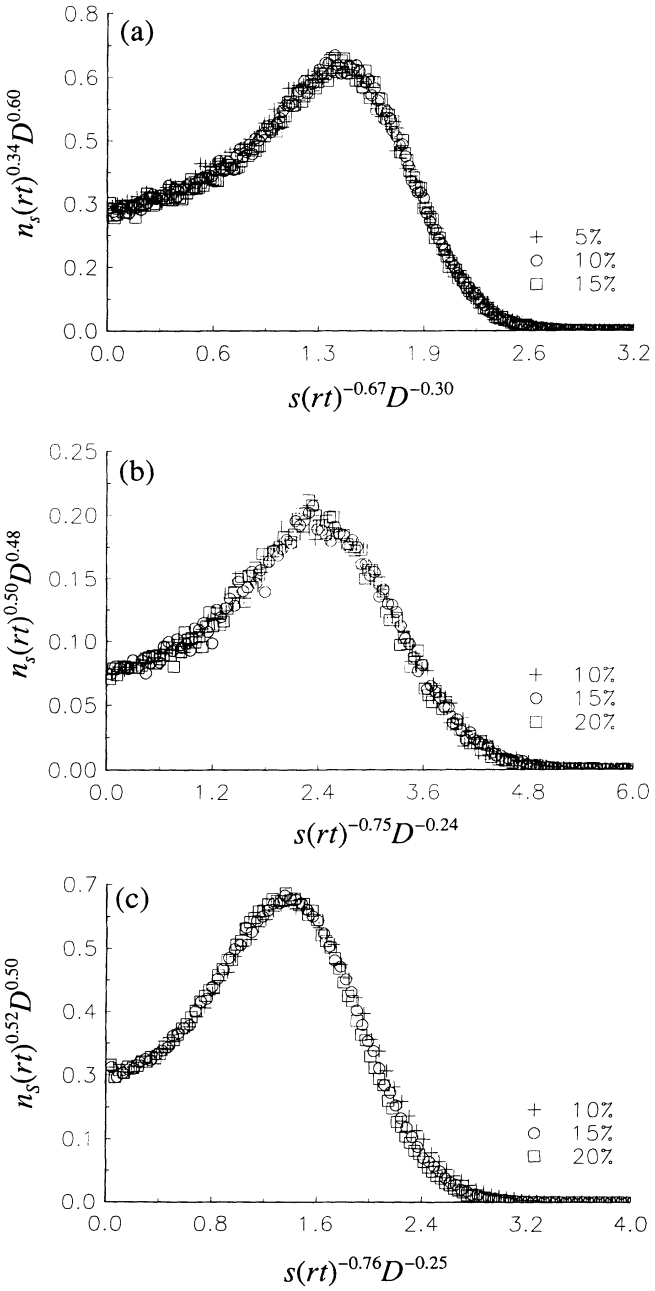

FIG. 8. Scaling of the island-size distribution in time, with $D = 10^8$, for (a) isotropic and (b) infinitely anisotropic diffusion, in two dimensions, and (c) one dimension.

Figure 4 explores the scaling of the walker density n with time. The data collapses for large t, as n is plotted against the variable $(rt)D$ for one-dimensional migration ($d_w = 1$), or $(rt)D^2$ for two-dimensional migration ($d_w = 2$). This is also the scaling behavior predicted by the rate equations (see Sec. VI). Similar collapse was found for the island density N in the variable rt/D. Figure 5 tests the scaling of $t_{\min}$ with D as derived in Appendix A. The $t_{\min}$ values in this figure were determined from the maxima of the walker density n since one expects scaling to set in rapidly after the maximum in the n vs t curves. The agreement with the predicted slope (see Table I for the simulation estimates of the exponents χ and ω) is extremely good even for such a "crude" assumption. Figure 6 shows the relationship between n and N, and suggests the asymptotic scaling relations $n(d_w = 1) \sim 1/(DN^2)$ and $n(d_w = 2) \sim 1/(DN)$, as are also obtained from the rate equations in Sec. VI.

In Figs. 7 and 8 we isolate the scaling of the island densities n_s with D from that with the coverage rt, respectively. The collapse of the data is fairly good and very sensitive to the exact choice of the effective exponents χ and φ. Uniformly good collapse is observed using the variable s/s_{av}. The simulation data are consistent with the existence of an asymptotic scaling function g which is analytic. This g would differ from the function associated with the rate equations (see Appendix C). Furthermore, the scaling function approaches a nonzero constant for small values of its argument, as is implicit in the scaling hypothesis (1). Results on the distribution of island separations are presented in detail in Sec. VII.

VI. THE RATE-EQUATION FORMULATION

Two key observations underlie our analysis of this process via "unconventional" rate equations: (i) the lifetimes τ for walkers to undergo nucleation (meeting other walkers) and aggregation (meeting islands) are comparable for large D (see Table II); (ii) the probability that a deposited atom nucleates rather than aggregates scales like $P \sim n/(n+N) \sim n/N \ll 1$, if $n \ll N$. One thus obtains the equations[6]

$$\frac{dN}{dt} = rn + \frac{n}{\tau} P \quad \text{and} \quad \frac{dn}{dt} = r(1-n) - \frac{n}{\tau} \ . \tag{5}$$

While (i) and (ii) apply for rather general dynamics of de-

posited atoms, we only elucidate their validity for random walks (RW) of relevance here. The space-filling property of $(d_w \leq 2)$-dimensional RW guarantees that walkers meet near, rather than distant, neighboring islands or walkers. Thus atoms must deposit in the "vicinity" of another walker for nucleation, which occurs with the small probability $P \sim n/N$. Furthermore, after short times, for both nucleation and aggregation lifetimes, $h_0\tau$ measures the average number of lattice steps for a RW to visit of the order $1/(n+N) \sim 1/N$ distinct sites associated with each island *or* walker. This contrasts the argument of Mo *et al.*[2] which assumes that a walker visits $1/n$ sites before nucleation. Recall that a two-dimensional isotropic random walk $(d_w = 2)$ between nearest-neighbor sites visits on average $\pi H/\ln H$ distinct sites after making H hops, for large enough H, while a one-dimensional random walk $(d_w = 1)$ visits only $(8H/\pi)^{1/2}$ distinct sites. For an average of $1/N$ sites visited, $H(d_w = 1) \approx \pi/(8N^2)$ and $H(d_w = 2) \approx 1/(\pi N)\ln(1/\pi N)$. Therefore $h_0\tau \sim \pi/8N^2$ and $\sim 1/\pi N$, respectively, for $d_w = 1$ and 2 (see Table II).

Numerical integration of (5) demonstrates that a quasistationary regime exists where $dn/dt \sim 0$. This further gives $n \sim r\tau$, for large D and $n \ll N$. Note that, through τ, the density n is a function of time, the quasistationary condition corresponding simply to the kinetic balance between deposition and aggregation events. Assuming $N \ll 1$ and D is large, so that logarithmic corrections are small (see Appendix B for more details), the important relations

$$n(d_w = 1) \simeq \frac{\pi}{8DN^2}$$

and (6)

$$n(d_w = 2) = \frac{1}{\pi DN}\ln\left[\frac{1}{\pi N}\right] \sim \frac{1}{\pi DN} ,$$

follow. They provide an additional relation among the exponents α, ω, χ, and φ, namely $\alpha = 2(\omega+1)/d_w$ and $\varphi = 1 - 2\chi/d_w$, for $d_w = 1, 2$. Substituting (6) in (5) yields asymptotically,

$$N \sim \left[\frac{\pi}{2}\left[\frac{rt}{D}\right]\right]^{1/4} \quad \text{and} \quad n \sim \left[\frac{32}{\pi}(rt)D\right]^{-1/2} \tag{7}$$

if $d_w = 1$, and

$$N \sim \left[\frac{3}{\pi}\left[\frac{rt}{D}\right]\right]^{1/3} \quad \text{and} \quad n \sim [3\pi^2(rt)D^2]^{-1/3} \tag{8}$$

if $d_w = 2$. The prefactors show a trend (from $d_w = 1$ to 2) similar to that found in the simulations, though their values are slightly different from the simulation estimates. Figure 9 shows refined estimates of χ, from the local slopes of $\log N$-$\log D$ plots obtained from numerical integration of (5). Similar dependence on the finite range of D was found in the simulation data, and arises from small-D corrections to scaling.

The logarithmic corrections in the lifetimes for isotropic diffusion are important to consider in practice, if the scaling results are to be used in estimating diffusion prefactors and energy barriers within the experimental error. They introduce corresponding corrections to scaling, e.g.,

$$N \sim (rt/D)^{1/3}[\ln(rt/D)]^{1/3} ,$$

which modify the effective exponents over the range $D \leq 10^8$. In Appendix B we derive the above solution and illustrate the order of the corrections expected. This is, of course, in addition to the corrections to the leading scaling behavior already present for the smaller values of D.

The above rate-equation formulation for the walker and island densities can be extended to characterize the full island-size distribution n_s for sizes $s \geq 1$. Rate equations for the n_s are usually called Smoluchowski equations. However, we emphasize that the form of the equations presented here is unconventional, necessarily reflecting the essential physics of this far-from-equilibrium deposition process. Let P_s denote the probability of deposition in the vicinity of an island of size s, so $P_s \sim n_s/(N+n) \sim n_s/N$ (for $n \ll N$), $P_1 = P$, and

TABLE II. Direct estimates of the average aggregation lifetimes, at fixed dose (5% for isotropic, and 10% for infinitely anisotropic and one-dimensional diffusion). τ_1 and τ_2 refer to the average simulation lifetimes for nucleation and growth, respectively, to be compared with the effective-rate equation lifetime τ (see text).

d	D	$r\tau_1$ (nucleation)	$r\tau_2$ (aggregation)	$r\tau$
1	10^4	2.0×10^{-2}	1.4×10^{-2}	5.6×10^{-2}
	10^6	1.6×10^{-3}	1.1×10^{-3}	1.9×10^{-3}
	10^8	7.2×10^{-5}	8.6×10^{-5}	1.2×10^{-4}
2 (anisotropic)	10^4	1.1×10^{-2}	8.2×10^{-3}	7.4×10^{-2}
	10^6	1.1×10^{-3}	6.3×10^{-3}	4.3×10^{-3}
	10^8	9.6×10^{-5}	5.6×10^{-4}	3.3×10^{-4}
2 (isotropic)	10^4	7.3×10^{-3}	5.2×10^{-3}	4.8×10^{-3}
	10^6	2.3×10^{-4}	3.9×10^{-4}	1.3×10^{-4}
	10^8	2.4×10^{-5}	1.5×10^{-5}	4.8×10^{-6}

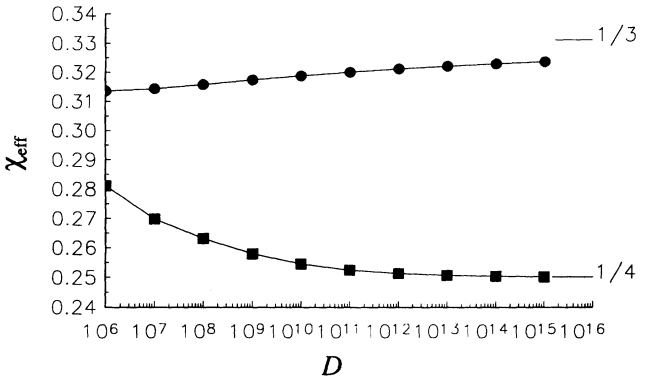

FIG. 9. The effective exponent $\chi_{\rm eff}$ obtained from the numerical solutions of the rate equations, in the range $D=10^6$–10^{15}, for isotropic (●, $rt=5\%$) and infinitely anisotropic (■, $rt=10\%$) diffusion.

$\sum_{s\geq 1} P_s = 1$. Accounting for all "two-body collisions," islands of size s can be created by deposition adjacent to or aggregation with an island of size $s-1$; likewise they can be removed by conversion to size $s+1$ islands through deposition or aggregation processes. Since the characteristic time for *all* aggregation processes is τ, specified above, we conclude that

$$\frac{dn_s}{dt} = rn_{s-1} - rn_s + \frac{n}{\tau}P_{s-1} - \frac{n}{\tau}P_s \quad \text{for } s \geq 2 \ . \tag{9}$$

The rate equation for $n_1 = n$ is as above, and applying $\sum_{s\geq 2}$ to (9) recovers the dN/dt equation.

The rate equations in (9) are amenable to analysis by a generating function approach. Since the most important terms in (9) arise from direct deposition of walkers and from island growth events, we first reduce these equations to

$$\frac{dn_{s\geq 2}}{dt} \approx Kn(n_{s-1} - n_s) \ ,$$
$$\frac{dn}{dt} \approx r - KNn \ . \tag{10}$$

Recall that, for $d_w = 1$, $K \sim 8h_0 N/\pi$,

$$n \sim [32(rt)D/\pi]^{-1/2} \ ,$$
$$N \sim [\pi(rt)/(2D)]^{1/4} \ ,$$

and

$$s_{\rm av} \sim \theta/N \sim [2(rt)^3 D/\pi]^{1/4} \ ,$$

whereas for $d_w = 2$, $K \sim \pi h_0$,

$$n \sim [3\pi^2 (rt)D^2]^{-1/3} \ ,$$
$$N \sim [3(rt)/(\pi D)]^{1/3} \ ,$$

and

$$s_{\rm av} \sim [\pi(rt)^2 D/3]^{1/3} \ .$$

We introduce the standard generating function

$$G(z,t) = \sum_{s=2}^{\infty} z^{s-2} n_s(t) \ , \tag{11}$$

from which the island-size densities can be recovered using

$$n_{s\geq 2} = [1/(s-2)!]\partial^{s-2} G(z=0,t)/\partial z^{s-2} \ .$$

Summing over all $s \geq 2$ in the rate equations one obtains

$$\frac{\partial}{\partial t} G(z,t) \approx Kn[n - (1-z)G(z,t)] \ , \tag{12}$$

with $G(z,t=0)=0$. The solution can be written trivially as

$$G(z,t) \approx \exp\left[-(1-z)\int_{\approx 0}^{t} du\, K(u)n(u)\right] \int_{\approx 0}^{t} du\, K(u)n^2(u) \exp\left[(1-z)\int_{\approx 0}^{u} dv\, K(v)n(v)\right] \ . \tag{13}$$

Substituting expressions for K, N, and n, and using $D = h_0/r$, yields

$$n_{s\geq 2}(d_w = 1) \approx \frac{1}{4(s-2)!} \int_{\approx 0}^{rt} du \left[\frac{\pi}{2Du^3}\right]^{1/4} \mathcal{E}\left\{\frac{4}{3}\left[\frac{2D(rt)^3}{\pi}\right]^{1/4}\left[1 - \left[\frac{u}{rt}\right]^{3/4}\right]\right\} , \tag{14}$$

and

$$n_{s\geq 2}(d_w = 2) \approx \frac{1}{(s-2)!} \int_{\approx 0}^{rt} \frac{du}{(9\pi D u^2)^{1/3}} \mathcal{E}\left\{\frac{1}{2}[9\pi D(rt)^2]^{1/3}\left[1 - \left[\frac{u}{rt}\right]^{2/3}\right]\right\} , \tag{15}$$

where $\mathcal{E}(x) = x^{s-2}\exp(-x)$. From these results, we extract the scaling functions g where

$$n_s \sim (rt)^{2\omega+1} D^{-2\chi} g(s/\bar{s})$$

and $\bar{s} = (\frac{4}{3})s_{\rm av}(d_w = 1)$ or $\bar{s} = (\frac{3}{2})s_{\rm av}(d_w = 2)$ (see Appendix C).

Setting $y = s/\bar{s}$, application of the method of steepest descents (see Appendix C for details) gives

$$g(0 \leq y < 1; d_w = 1) = \frac{1}{4}\left[\frac{\pi}{2}\right]^{1/2} (1-y)^{-2/3} \ , \tag{16}$$

and

$$g(0 \leq y < 1; d_w = 2) = \frac{3}{(9\pi)^{2/3}} (1-y)^{-1/2} \ , \tag{17}$$

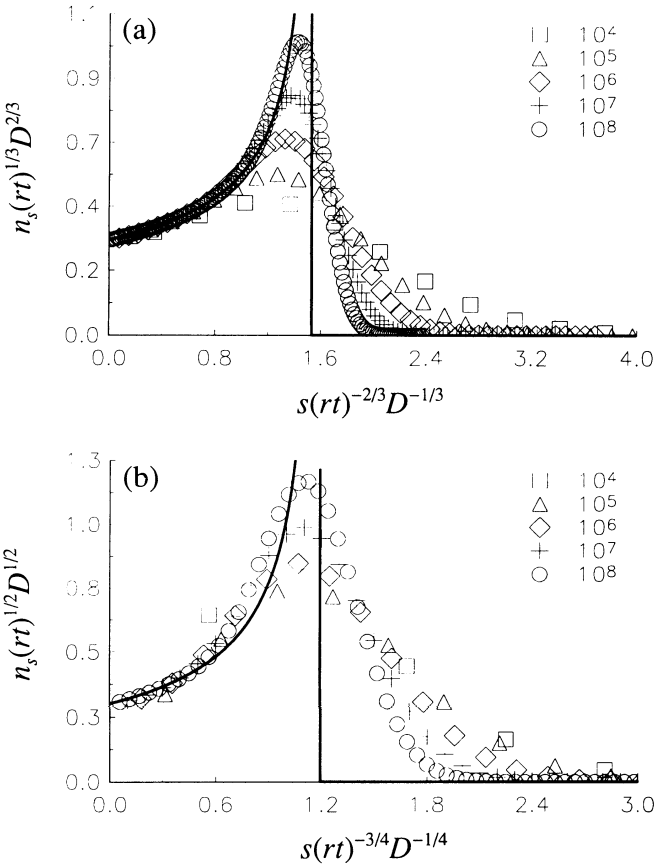

FIG. 10. The scaled island-size densities $n_s(rt)^{-(2\omega+1)}D^{2\chi}$, at fixed dose, as functions of the scaled size $s(rt)^{\omega}D^{-\chi}$ for (a) isotropic ($rt=5\%$) and (b) infinitely anisotropic diffusion ($rt=10\%$). The solid line is the fit provided by the solution derived in detail in Appendix C. Identical collapse and analytic fit is obtained at fixed diffusion ratio but variable dose.

while $g(y>1)=0$, for both values of d_w. In addition, the rate equations predict $g(0;d_w=1)=0.313\,328\,5\ldots$, and $g(0;d_w=2)=0.323\,240\,9\ldots$. Figure 10 overlaps the results of numerical integration of the equations in (10) with the scaling functions g above.

VII. DISTRIBUTION OF ISLAND SEPARATIONS

In this section we want to address a few of the issues regarding the spatial distribution of islands. This distribution contains features difficult to incorporate in a simple rate-equation treatment, but also important additional information. Of interest, e.g., are possible deviations from a random (Poisson) distribution of islands on the surface, especially at small island separations, where competition for incoming walkers can introduce nontrivial island-island or island-walker correlations, in size and separations. Analogously, one could analyze the distribution of island separations to first, second, etc. neighbors, or the distribution of island distances from an arbitrary empty site on the surface—this being the distribution of distances probed by the walkers during migration on the surface.[20] Here we restrict our attention to the island pair-correlation function, and just in the case of isotropic diffusion in two dimensions. We expect similar conclusions in the case of anisotropic diffusion. At low coverages, one can define a characteristic separation between islands, $R_{av}\sim(1/N)^{1/2}$, with which one expects all characteristic distances to scale. At low coverages, one can define a characteristic separation between islands, $R_{av}\sim(1/N)^{1/2}$, with which one expects all characteristic distances to scale. The aim, then, is to obtain information about the depletion of the concentration of island pairs at short distances (compared to R_{av}), to examine the crossover to the large-separation behavior, and to demonstrate scaling with R_{av}.

Let $N(\mathbf{r})$ denote the conditional probability of finding an island (of *any* size) at the position $\mathbf{r}$ (in lattice vectors), relative to another island (also of any size). In the absence of long-range order, clearly $N(\mathbf{r})\rightarrow N$, as $|\mathbf{r}|\rightarrow\infty$, regardless of the direction. As $D\rightarrow\infty$, the characteristic separation, R_{av}, becomes very large compared to the lattice spacing, and quantities defined in terms of distances measured in units of R_{av} vary smoothly and become isotropic. We postulate the following scaling relation for the pair probability:

$$N(\mathbf{r})\sim Nf\left(\frac{|\mathbf{r}|}{R_{av}}\right), \tag{18}$$

where $f(0)=0$, $f(x\rightarrow\infty)\rightarrow 1$.

In the simulations it is straightforward to determine the total number $\Omega(R)$ of *distinct* island pairs at a given distance R for fixed coverage and diffusion ratio. Since we are adsorbing on a square lattice, the total number $M(R)$ of different possible sites on the lattice a given distance R from an origin [in other words, the number of distinct pairs of integers (i,j) with $i^2+j^2=R^2$] is almost always 8 if nonzero. The exact formula for $M(R)$ is available (see, e.g., Ref. 21). In Fig. 11 we plot the rotationally averaged $N(\mathbf{r})$, given by

$$\Omega(|\mathbf{r}|)/[M(|\mathbf{r}|)NL^2],$$

for a $L\times L$ square lattice.

In a manner entirely analogous to our formulation of the rate equations for the total average island density, one can construct effective rate equations for $N(\mathbf{r})$, for $|\mathbf{r}|\ll R_{av}$. Note that the quantity $N(\mathbf{r})$, with $|\mathbf{r}|<R_{av}$, will increase whenever two walkers succeed at meeting at such a "short distance" from an existing island *before* they aggregate with that island. Clearly, this must be increasingly more difficult as $|\mathbf{r}|$ decreases. First denote the density of walkers already on the lattice a distance $O(|\mathbf{r}|)$ from an island by

$$n_r\sim n\gamma(\mathbf{r}),$$

where $\gamma(\mathbf{r})$ accounts for any depletion of the walker density due to the nearby island "sink." The probability for another walker to land within a distance $O(|\mathbf{r}|)$ of such a walker is

$$P_r=(|\mathbf{r}|/R_{av})^2[n\gamma(\mathbf{r})/N].$$

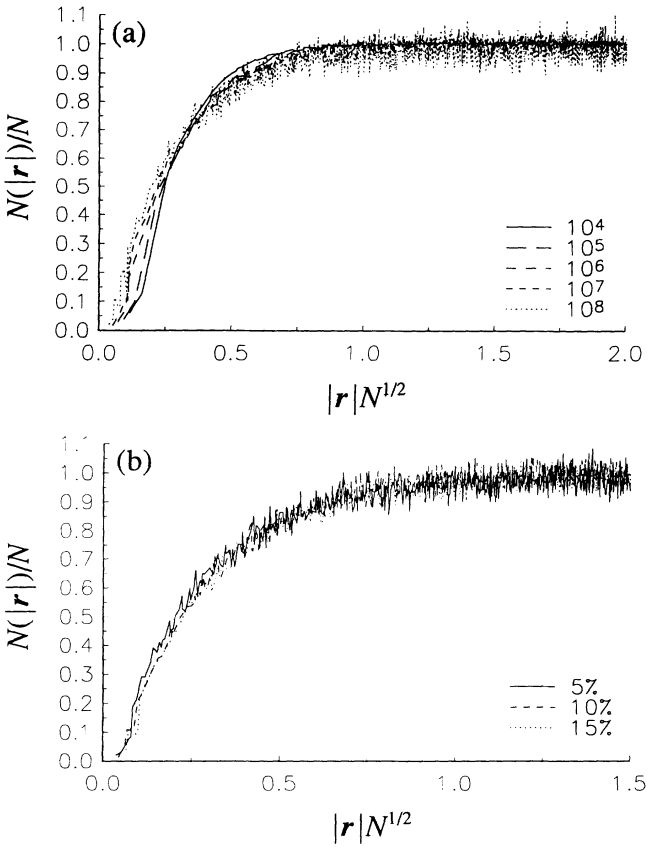

FIG. 11. (a) The rotationally averaged conditional probability $N(|\mathbf{r}|)$, normalized by the total density of islands N (see text) and plotted against the scaling variable $|\mathbf{r}|/R_{\rm av} \sim |\mathbf{r}|N^{1/2}$ for $rt = 5\%$. (b) The same as (a) but at fixed diffusion ratio $D = 10^8$, and variable dose.

The lifetime of such a walker is reduced to $\tau_r \sim (|\mathbf{r}|/R_{\rm av})^2\tau$. Thus, the rate equation for $N(\mathbf{r})$, with $|\mathbf{r}| \ll R_{\rm av}$, has the form

$$\frac{dN(\mathbf{r})}{dt} \sim \frac{n_r}{\tau_r} P_r \sim \frac{n}{\tau}\left[\frac{n}{N}\right]\gamma(\mathbf{r})^2 , \tag{19}$$

which, combined with (6)–(8), yields

$$N(\mathbf{r}) \sim (rt/D)^{1/3}\gamma(\mathbf{r})^2 \sim \gamma(\mathbf{r})^2 N .$$

Close examination of our simulation data in the small-x region reveals behavior consistent with this dependence which agrees with the prediction of previous formulations.[3] As $|\mathbf{r}|$ gets large, the typical distance from a walker at $\mathbf{r}$ to the nearest island becomes of the order of $R_{\rm av} \sim N^{-1/2}$, and one recovers the behavior of the average quantities, i.e., $dN(\mathbf{r})/dt \to dN/dt$.

Finally, note that much more detailed information on the island distribution is available in the probabilities $N_{s,s'}(\mathbf{r})$ for finding and island of size s separated by $\mathbf{r}$ from an island of size s'. Note that the $N_{s,s'}(\mathbf{r})$ determine the diffraction profile. As $|\mathbf{r}| \to \infty$, one should again recover the average uncorrelated behavior, i.e.,

$$N_{s,s'}(\mathbf{r}) \to N_{s,s'}(|\mathbf{r}|) \sim n_s n_{s'} .$$

For finite $|\mathbf{r}|$, one naturally compares $N_{s,s'}(\mathbf{r})$ with $n_s n_{s'} N(\mathbf{r})/N$. Should one expect

$$N_{s,s'}(\mathbf{r}) < n_s n_{s'} N(\mathbf{r})/N ,$$

for $s, s' \gg s_{\rm av}$, due to competition of oversized islands for walkers? Further numerical and analytical work on this issue is in progress and will be presented elsewhere.[20]

VIII. CONCLUSIONS

In conclusion, we present here Monte Carlo results for the analytic dependence of the island and walker densities, and the distribution of island sizes and separations, on the coverage and on the ratio of diffusion to deposition rates, for submonolayer irreversible island formation. A rate-equation approach is also developed for the average densities and complete island-size distribution. Knowledge of the scaling functions for the distribution of island sizes provides further opportunity to check the theory against experimental data. The effective rate equations incorporate the equivalence of the walker lifetimes for aggregation to other walkers *or* to islands, a key feature of the model at low coverages (but above those of the transient regime). Generally, the rate-equation treatment provides a fairly good description of the nucleation and growth kinetics of our model, mostly qualitatively correct. This suggests that for the average quantities, of experimental interest, the effects of fluctuations in the growth rates, high-order correlations, and corrections towards the true distribution of walker lifetimes are weak. Interestingly, the rate equations yield a nonanalytic scaling function for the island-size distribution, identically zero above some cutoff. Nonanalyticity of the scaling function is not clear from the simulation data, though a slower approach to nonanalyticity cannot be entirely ruled out. Preliminary results are discussed for the distribution of island separations. We emphasize the depletion in the concentration of island pairs at small distances. Investigation of finite diffusion anisotropies is also relevant, and is addressed in a separate report.[22]

ACKNOWLEDGMENTS

We would like to acknowledge discussions with Professor Michael Tringides and thank Maria de Fátima Carvalho and Paulo Ventura for pointing out the results in Ref. 21. Our work was supported by the National Science Foundation Grant No. CHE-9014214, and was performed at Ames Laboratory. Ames Laboratory is operated for the U.S. Department of Energy by Iowa State University under Contract No. W-7405-Eng-82.

APPENDIX A: THE TIME RANGE FOR SCALING

Here we use the scaling relations for $n \sim (rt)^{-\alpha} D^{-\varphi}$, $N \sim (rt)^{\omega+1} D^{-\chi}$, and $\tau \sim 1/(DN^{2/d_w})$, for $d_w = 1$ or 2, to analyze contributions to the rate dn/dt in (5), whose

dominant terms come from deposition events and aggregation of walkers to islands. It follows that the quasistationary condition $dn/dt \approx 0$, which means effectively $|dn/dt| \ll \{r, n/\tau\}$, implies

$$(rt)^{-\alpha-1}D^{-\varphi} \ll \{1,(rt)^{-\alpha+2(\omega+1)/d_w} \times D^{1-\varphi-2\chi/d_w}\} ,$$

for $d_w = 1,2$, or

$$rt \gg \{D^{-\varphi/(\alpha+1)}, D^{-(d_w-2\chi)/[d_w+2(\omega+1)]}\} .$$

Given the scaling relations among α, ω, φ, and χ (see Secs. IV and VI), one gets simply $rt_{\min} \sim D^{-|\chi/\omega|}$. For $d_w = 1$, $rt_{\min} \sim D^{-1/3}$, while for $d_w = 2$, $rt_{\min} \sim D^{-1/2}$. In practice, for $rt \approx 5-10\%$, the scaling regime should set in as $D \gg 10^2 - 10^3$.

The question of whether there is an upper dose limit, beyond which the scaling as postulated in (1) and (4) no longer holds is related to reaching finite densities of islands at which the interisland separation becomes of the order of a few lattice spacings. Thus, the condition to look for is basically $1/N \gg 1$, that is, $(rt)^{\omega+1}D^{-\chi} \ll 1$, or $rt \ll D^{\chi/(\omega+1)}$. This means, effectively, $rt \ll D$ for both $d_w = 1$ and 2. The full time range reads, then, as

$$D^{-|\chi/\omega|} \ll rt \ll D^{\chi/(\omega+1)} .$$

In real systems, where islands have finite extent, the cutoff will occur much earlier, for $\theta = O(1)$, as noted before in the text. In our model, the scaling form should certainly apply for θ not in excess of 10–20%.

APPENDIX B: LOGARITHMIC CORRECTIONS IN THE RATE EQUATIONS

For an isotropic random walk on a two-dimensional square lattice (of unit lattice spacing), the average number of hops H to visit $1/N$ distinct sites, satisfies approximately (for large H)

$$\frac{1}{N} = \frac{\pi H}{\ln H} .$$

Inverting this relation in order to solve recursively for H gives

$$H = \frac{\ln H}{\pi N} = \frac{1}{\pi N}\ln\left[\frac{1}{\pi N}\ln H\right] = \frac{1}{\pi N}\left[\ln\frac{1}{\pi N} + O\left[\ln\ln\frac{1}{\pi N}\right]\right] .$$

If h_0 and τ denote the hopping rate and average lifetime of a walker, respectively, then $H = h_0\tau$. Recall that $n = r\tau$. Substituting the leading expression for τ, as a function of N and h_0, in the rate equation for N gives

$$\frac{dN}{d(rt)} = n + \frac{n}{r\tau}\left[\frac{n}{N}\right] \approx \frac{1}{\pi DN}\ln\frac{1}{\pi N} + \frac{1}{\pi DN^2}\ln\frac{1}{\pi N} ,$$

with $D = h_0/r$. For $N \ll 1$, the second term on the right-hand side clearly dominates the asymptotic scaling, and one obtains $N \sim (3rt/\pi D)^{1/3}$. However, one can easily extract the leading corrections in a standard way. The above rate equation is separable in the variables N and t. We can then solve for N, keeping only the leading logarithmic correction, for $N \ll 1$. The result is

$$N \sim \left[\frac{3rt}{\pi D}\right]^{1/3}\left[\ln\frac{1}{\pi(3rt/\pi D)^{1/3}}\right]^{1/3} .$$

For $rt = 10\%$ and $D = 10^8$, applying logarithms to both sides, one gets an effective exponent of 0.30, consistent with the values below $\frac{1}{3}$ always found in the simulations (see Table I) and in the numerical integration of the rate equations. This 10% deviation from the asymptotic $\frac{1}{3}$ value decreases very slowly with increasing D, however. At $D = 10^{20}$ it is still about 5%.

APPENDIX C: SOLUTIONS OF THE RATE EQUATIONS

In this appendix we give details on obtaining the asymptotic solution of the rate equations for the island-size densities $n_{s\geq 2}$. Since the mean-field limit does not distinguish the substrate dimensionality, we have only to examine two cases: $d_w = 1$ and 2. We will work simply with the dominant rate terms (corresponding to the most common events for large D) on the right-hand side of (9).

1. Scaling limit $D \to \infty$: Region $s < \bar{s}$ $(0 \leq y < 1)$

Case 1: $d_w = 1$. In (14) it is convenient to change to an integration variable

$$v = (\tfrac{4}{3})[2D(rt)^3/\pi]^{1/4}\{1-[u/(rt)]^{3/4}\} ,$$

in terms of which

$$n_{s\geq 2} = \frac{1}{(s-2)!}\int_0^{4/3[2D(rt)^3/\pi]^{1/4}} dv \frac{1}{4}\left[\frac{\pi}{2D(rt)}\right]^{1/2}\left[1-\frac{3}{4}\left[\frac{\pi}{2D(rt)^3}\right]^{1/4} v\right]^{-2/3} v^{s-2}\exp(-v) .$$

Using the notation, $\bar{s} = 4[2D(rt)^3/\pi]^{1/4}/3 \sim (\frac{4}{3})s_{\rm av}$,

$$n_{s\geq 2}D^{1/2}(rt)^{1/2} \sim g(s/\bar{s}) \approx \frac{1}{4}\left[\frac{\pi}{2}\right]^{1/2}\frac{1}{(s-2)!}\int_0^{\bar{s}} dv\left[1-\frac{v}{\bar{s}}\right]^{-2/3} v^{s-2}\exp(-v) .$$

The aim is to verify now the dependence of g on the unique variable $y=s/\bar{s}$, as postulated in (1). In terms of y, with the substitution $w=v/(y\bar{s})$, and the approximation

$$(s-2)!\approx s!\approx(2\pi s)^{1/2}s^s e^{-s} ,$$

one obtains

$$g(y)\approx\frac{1}{8}\sqrt{y\bar{s}}\int_0^{1/y} dw\, e^{y\bar{s}(1-w+\ln w)}(1-yw)^{-2/3} .$$

In the scaling limit $D\to\infty$, $s_{\rm av}$ (and $\bar{s}$) is a large parameter and the integrand is already in a form suitable for application of the method of steepest descents. The saddle point occurs at $w=1$, for $0\le y<1$, (i.e., $s<\bar{s}$). One thus obtains

$$g(0\le y<1)\approx\frac{1}{4}\left[\frac{\pi}{2}\right]^{1/2}(1-y)^{-2/3} .$$

Case 2: $d_w=2$. The change of integration variables to $v=[9\pi D(rt)^2]^{1/3}\{1-[u/(rt)]^{2/3}\}$, in (15), reduces the expression for the n_s in this case to

$$n_{s\ge 2}\approx\frac{1}{(s-2)!}\int_0^{1/2[9\pi D(rt)^2]^{1/3}} dv\frac{3}{[(9\pi D)^2(rt)]^{1/3}}\left[1-\frac{2v}{[9\pi D(rt)^2]^{1/3}}\right]^{-1/2} v^{s-2}\exp(-v) .$$

If we define now $\bar{s}=[9\pi D(rt)^2]^{1/3}/2\sim(3/2)s_{\rm av}$, $y=s/\bar{s}$, $w=v/(y\bar{s})$, and using again Stirling's approximation,

$$n_{s\ge 2}D^{2/3}(rt)^{1/3}\sim g(y)\approx\frac{3}{(9\pi)^{2/3}}\left[\frac{y\bar{s}}{2\pi}\right]^{1/2}\int_0^{1/y} dw\, e^{y\bar{s}(1-w+\ln w)}(1-yw)^{-1/2} ,$$

and finally,

$$g(0\le y<1)\approx\frac{3}{(9\pi)^{2/3}}(1-y)^{-1/2} .$$

2. Scaling limit $D\to\infty$: Region $s>\bar{s}$ (i.e., $y>1$)

Cases 1 and 2: $d_w=1,2$. When $y>1$, the main contribution to the integral in $g(y)$ comes from the region around the upper limit, $z\approx 1/y$, and has the form

$$g(y)\propto\left[\frac{\bar{s}}{y}\right]^{1/2} e^{y\bar{s}[1-(1/y)+\ln(1/y)]}\underset{(D\to\infty)}{\to}0 ,$$

since $1-1/y+\ln(1/y)\le 0$. Thus for both cases, $d_w=1$ or 2, the function $g(y)=0$, for $y>1$.

---

[1] Y. W. Mo, J. Kleiner, M. B. Webb, and M. G. Lagally, Phys. Rev. Lett. **66**, 1998 (1991).

[2] R. Q. Hwang, J. Schröder, C. Günter, and R. J. Behm, Phys. Rev. Lett. **67**, 3279 (1991).

[3] J. A. Venables, G. D. Spiller, and M. Handbücken, Rep. Prog. Phys. **47**, 399 (1984).

[4] J. D. Weeks and G. H. Gilmer, Adv. Chem. Phys. **40**, 157 (1979).

[5] J. W. Evans, in *Structure of Surfaces III,* edited by S. Y. Tong *et al.* (Springer, Berlin, 1991).

[6] M. C. Bartelt, M. C. Tringides, and J. W. Evans (unpublished).

[7] A. F. Voter, Phys. Rev. B **34**, 6819 (1986); Proc. SPIE **821**, 214 (1987).

[8] G. Comsa, Bull. Am. Phys. Soc. **37**, 106 (1992).

[9] T. A. Witten and L. M. Sander, Phys. Rev. Lett. **47**, 1400 (1981).

[10] J. W. Evans, Phys. Rev. A **40**, RC2868 (1989).

[11] E. S. Hood, B. H. Toby, and W. H. Weinberg, Phys. Rev. Lett. **55**, 2437 (1985).

[12] D. E. Sanders and J. W. Evans, Phys. Rev. A **38**, 4186 (1988); J. W. Evans, R. S. Nord, and J. A. Rabaey, Phys. Rev. B **37**, 8598 (1988).

[13] A. Getis and B. Boots, *Models of Spatial Processes* (Cambridge University Press, Cambridge, England, 1978).

[14] P. Meakin, Rep. Prog. Phys. **55**, 157 (1992), and references therein.

[15] D. Stauffer, Phys. Rep. **54**, 1 (1979).

[16] J. A. Blackman and A. Wilding, Europhys. Lett. **16**, 115 (1991).

[17] G. Brocks, P. J. Kelly, and R. Car, Phys. Rev. Lett. **66**, 1729 (1991).

[18] Z. Zhang, Y.-T. Lu, and H. Metiu, Surf. Sci. **255**, L543 (1991).

[19] P. A. Thiel and T. E. Madey, Surf. Sci. Rep. **7**, 211 (1987).

[20] M. C. Bartelt and J. W. Evans (unpublished).

[21] G. H. Hardy and E. M. Wright, *An Introduction to the Theory of Numbers* (Clarendon, Oxford, 1938), p. 241.

[22] M. C. Bartelt and J. W. Evans, Europhys. Lett. (to be published).